

Wet granular walkers and climbers

This content has been downloaded from IOPscience. Please scroll down to see the full text.

2011 New J. Phys. 13 053041

(<http://iopscience.iop.org/1367-2630/13/5/053041>)

View [the table of contents for this issue](#), or go to the [journal homepage](#) for more

Download details:

IP Address: 140.77.240.25

This content was downloaded on 29/01/2014 at 14:26

Please note that [terms and conditions apply](#).

Wet granular walkers and climbers

Z S Khan¹, A Steinberger^{1,2,4}, R Seemann^{1,3}
and S Herminghaus¹

¹ Max Planck Institute for Dynamics and Self-Organization, Bunsenstrasse 10,
D-37073 Göttingen, Germany

² Laboratoire de Physique, Ecole Normale Supérieure de Lyon, CNRS UMR
5672, Université de Lyon, 46 Allée d'Italie, F-69364 Lyon, France

³ Experimental Physics, Saarland University, Postfach 151 150, Gebäude C6.3,
D-66041 Saarbrücken, Germany

E-mail: audrey.steinberger@ens-lyon.fr

New Journal of Physics **13** (2011) 053041 (15pp)

Received 27 September 2010

Published 24 May 2011

Online at <http://www.njp.org/>

doi:10.1088/1367-2630/13/5/053041

Abstract. Mechanisms of locomotion in microscopic systems are of great interest not only for technological applications but also for the sake of understanding, and potentially harnessing, processes far from thermal equilibrium. Downscaling is a particular challenge and has led to a number of interesting concepts, including thermal ratchet systems and asymmetric swimmers. Here we present a granular ratchet system employing a particularly robust mechanism that can be implemented in various settings. The system consists of wetted spheres of different sizes that adhere to each other, and are subject to a symmetric oscillating, zero average external force field. An inherent asymmetry in the mutual force network leads to force rectification and hence to locomotion. We present a simple model that accounts for the observed behaviour, underscores its robustness and suggests a potential scalability of the concept.

 Online supplementary data available from stacks.iop.org/NJP/13/053041/mmedia

⁴ Author to whom any correspondence should be addressed.

Contents

1. Introduction	2
2. Experimental results	2
3. Theoretical model	5
4. Discussion	11
5. Conclusion	14
Acknowledgments	14
References	15

1. Introduction

Interest in small-scale locomotion in biological systems, such as ciliates, flagellates, and molecular motors, has spurred a number of attempts to construct artificial devices characterized by similar merits [1–7]. The interest in achieving the long-range-directed motion of cells has led to the realization of directed cell migration using periodic asymmetric ratchet potentials via the surface patterning of cell-adhering regions [8]. Systems of particles in fluid dynamics settings can exhibit directed motion under periodic and symmetric forcing through the symmetry breaking of surface or streaming flows [2, 3]. Additionally, the controlled transport of particles and structures can be used for applications such as targeted delivery and stirring in lab-on-a-chip devices [2, 9, 10]. Dry frictional particles are known to ratchet under asymmetric vibration [11]. Aspherical particles with complex interactions have also been shown to convert periodic and symmetric external forces into net locomotion [12–14]. Here we report the discovery of a strikingly robust ratchet system that self-assembles in proper environments and self-aligns in the direction of the excitation, and we present a simple model of the system that reproduces the observed behaviour and infers a novel ratchet mechanism for the motion.

When a bidisperse mixture of glass beads is moistened by a fluid and shaken vertically and sinusoidally, small clusters of beads occasionally take off from the surface of the pile and rapidly climb up the container walls *against gravity*. Figure 1(a) and supplementary movie S1 (available from stacks.iop.org/NJP/13/053041/mmedia) demonstrate this effect where a cluster of beads spontaneously formed and climbed out of a pile of glass spheres (from Whitehouse Scientific, density $\rho = 2.5 \text{ g cm}^{-3}$) wetted 1% by total volume with a glycerol–water mixture (glycerol 87% from Merck, surface tension $\gamma = 61 \pm 1 \text{ mN m}^{-1}$ and viscosity $\eta = 0.12 \pm 0.01 \text{ Pa s}$). The upper surface of the granular pile can be seen as the dark region at the bottom of the images. These ‘climbers’ are held together and against the wall by capillary bridges; they are led by a large bead with one or more small beads trailing below. In this system, the self-assembly of these structures is assisted by the Brazil nut effect [15], as the large beads are transported to the top of the pile under vertical vibration. Many different ascending clusters have been observed, which differed in the number of spheres involved. This effect is robust, as we have observed it using numerous different wetting liquids (silicone oil, glycerol–water mixtures, ethylene glycol), container materials (glass and polystyrene) and geometries (cylindrical, rectangular).

2. Experimental results

In order to investigate the clusters’ locomotion, we have reproduced this effect in a simplified setting with artificially assembled clusters of precision ruby spheres (from Sandoz Fils SA,

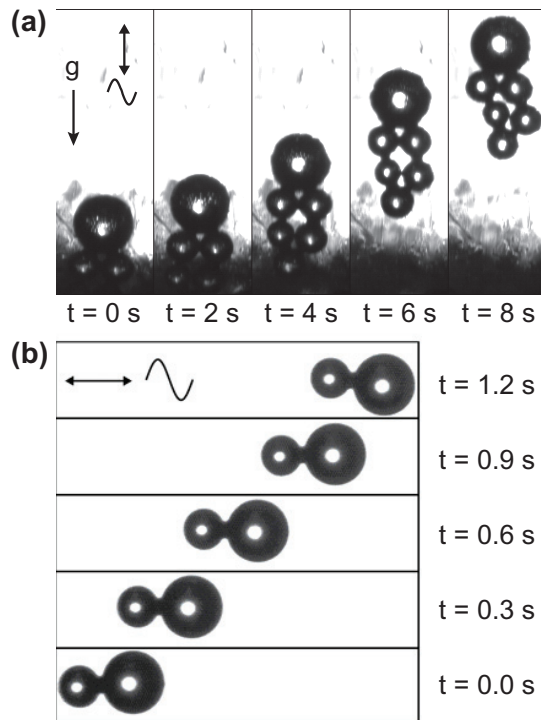


Figure 1. Time series of ratcheting structures. (a) Self-assembled structure from a 50 : 50 mixture of glass spheres with radii in the size ranges of 0.3–0.315 mm and 0.5–0.59 mm, migrating up the sidewall of a rectangular polystyrene container (10.6 mm long and wide, 44.8 mm high, from VWR International GmbH) under a vertical sinusoidal vibration with a frequency $f = 170$ Hz and a peak acceleration $a_0 = 16.2$ g (see supplementary movie S1). The sample was wetted 1% by volume with a glycerol–water mixture. The pile of grains is visible as the dark region at the bottom of the images. (b) Artificially assembled walker, composed of precision ruby spheres with 0.2 and 0.3 mm radii, migrating along the axis of vibration of a horizontally aligned silicone oil wetted glass microscope slide shaken at $f = 80$ Hz and $a_0 = 4$ g (see supplementary movie S2 available from stacks.iop.org/NJP/13/053041/mmedia).

density $\rho = 4.0 \text{ g cm}^{-3}$) on a horizontally aligned substrate. We focused our study on the simplest structure: an asymmetric dimer built out of one large and one small bead, which we call a walker. The substrate was aligned horizontally so that the effect of gravity on the walkers' motion can be neglected. It was either a Marienfeld glass microscope slide (76 mm long, 26 mm wide and 1 mm thick) or a 90° glass prism with a 25 mm-wide square face. The glass substrate was coated with a 4–5 nm-thick layer of chromium (using a BOC Edwards Auto 306 Evaporation System) to eliminate static charging effects on the moving clusters of spheres. We used silicone oil as a wetting fluid, as it is a perfectly wetting fluid for the substrate and the spheres and its evaporation can be neglected on the experimental timescales due to its low vapour pressure. The substrates were wetted with a 4–6 μm -thick layer of filtered Wacker silicone oil Si AK 5 (surface tension $\gamma = 19.2 \text{ mN m}^{-1}$, dynamic viscosity $\eta = 4.6 \text{ mPa s}$) prior to the experiments. A horizontal harmonic vibration was applied to the substrate using an

electromagnetic shaker (LDS model V406), such that the acceleration of the substrate is given by $a(t) = a_0 \cos(2\pi ft)$, where a_0 is the peak acceleration and f is the shaking frequency. The acceleration was monitored using a triple-axis accelerometer (Kistler model 8690C50), and we ensured that the unwanted acceleration in the vertical direction was below 3% of the driving acceleration.

The motion of the clusters was recorded with a PCO 1200hs CMOS camera mounted on a Zeiss Stemi 2000 C stereo microscope with a $0.63\times$ front lens. The time interval between successive pictures was set to an integer number of vibrations, typically one image per shake or one image every ten shakes, so that the substrate appeared immobile in the time series of pictures. We observed that the walkers aligned with the axis of vibration of the substrate as soon as the vibration was applied, and migrated in the direction of the larger sphere. The walkers travelled with a constant speed when viewed stroboscopically; one example of this motion is shown in figure 1(b) and supplementary movie S2. In order to obtain velocity measurements from the recorded time series, the position of the centroids of the structure was first determined in each image using the particle analysis package of ImageJ software, after isolating the structure from the background by applying a single threshold to the stack of pictures. The time series of structure positions was then further analysed using Matlab software.

Figure 2 shows experimental measurements of the walkers' velocity for vibration frequencies f from 60 to 90 Hz (symbols) against the peak acceleration a_0 of the horizontal vibration, for a walker with $R_1 = 0.3$ mm and $R_2 = 0.2$ mm. The walkers' locomotion velocities were obtained by averaging a minimum of six runs, where half of the measurements were done with the large sphere facing to the left and half with the large sphere facing to the right. Both locomotion directions along the axis of vibration were thereby sampled, thus ruling out the possible influence of any residual tilt of the set-up. The size of our experimental errors corresponds to the difference between the largest and smallest velocity measurements; they represent the dispersion of the velocities, presumably due to the presence of dust or irregularities on the surfaces.

We observed a nonlinear dependence of the walkers' locomotion velocity on the peak acceleration a_0 ; this rises sharply as the acceleration increases until it reaches a plateau near $a_0 \approx 6$ g (where $1 \text{ g} = 9.8 \text{ m s}^{-2}$), then drops off above $a_0 = 11$ g. Additionally, the data exhibit no significant frequency dependence, unlike dry frictional ratchet systems [12–14]. This suggests that the ratio of the applied force to the cohesive force is a relevant control parameter, as opposed to an energy ratio that would imply a dependence on the peak velocity of the substrate, $a_0/2\pi f$ [16]. For the following data analysis, we therefore introduce the dimensionless force Γ as the ratio between the inertial force acting on the structure and the average capillary force between the beads and the substrate. For a perfectly wetting liquid such as silicone oil, $\Gamma(t) = a(t)M/4\pi\gamma\bar{R}$, where M is the sum of the masses of the spheres, \bar{R} is the arithmetic mean of their radii and γ is the surface tension of the wetting fluid [17, 18]. We denote Γ_0 as the dimensionless peak force $a_0M/4\pi\gamma\bar{R}$. The inset of figure 2 shows that the minimum dimensionless peak force required for locomotion to occur, Γ_c , is also independent of the vibration frequency within the experimental uncertainties. The range of vibration frequencies used in the inset is representative of the limits of our experimental apparatus. Our shaker cannot perform well-controlled sinusoidal vibrations outside of this range as the motion of the substrate is dominated by the vibration eigenmodes of the set-up.

As the degree of asymmetry is a relevant control parameter for ratchet systems [1, 3, 13], we expect that the asymmetry of the walker would have an effect on its migration velocity. We

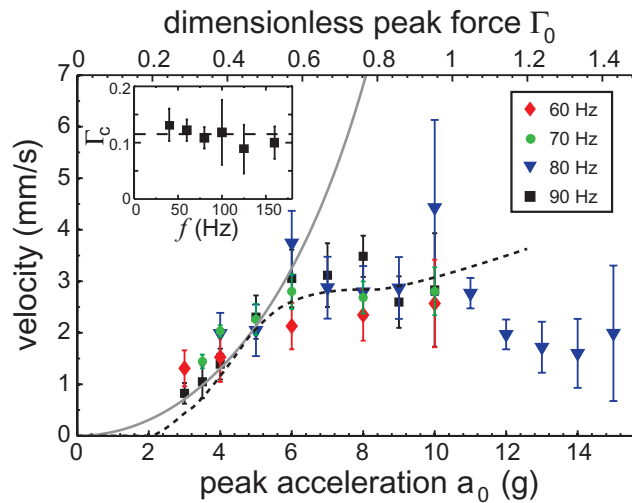


Figure 2. Measurements of the walkers' velocity as a function of the peak substrate acceleration a_0 (lower axis) and dimensionless peak force Γ_0 (upper axis) for different vibration frequencies f (see legend). These data were obtained for a walker with $R_1 = 0.3$ mm and $R_2 = 0.2$ mm ($\sin \delta = 0.2$) on a glass slide. The solid grey curve represents a fit of the average walker velocity calculated using a linear friction law to the experimental data where the coefficient of sliding friction, $\kappa = 0.032$ s mm $^{-1}$, is the only fit parameter (theory supplement, equation (S9), available from stacks.iop.org/NJP/13/053041/mmedia). The dashed black curve represents the expected average velocity for a friction law with a Coulomb and a viscous friction term, computed numerically with $\mu = 0.24$ and $\alpha = 550$. Inset: the dimensionless force at the onset of motion, Γ_c , as a function of the vibration frequency f . Γ_c was measured by gradually decreasing the peak plate acceleration a_0 and waiting for the walker to stop moving. The dashed line in the inset is located at the mean value of Γ_c . These experiments were performed on a glass prism. The error bars represent the range of data resulting from multiple experimental measurements.

characterize the asymmetry by the angle δ formed between the centres of the spheres and the horizontal, as shown schematically in the inset of figure 3. The main panel of figure 3 shows the velocity of the walkers as a function of the asymmetry parameter $\sin \delta = (R_1 - R_2)/(R_1 + R_2)$, measured with a fixed dimensionless peak force $\Gamma_0 = 0.5$ (solid symbols). The velocity vanishes in the case of symmetric walkers composed of spheres with identical radii ($\delta = 0$) on a well-levelled substrate, and increases with the degree of asymmetry, $\sin \delta$.

3. Theoretical model

Having identified the relevant parameters, we present a simple model to explain our experimental observations and to elucidate the mechanism of locomotion. We show that directed motion arises from the asymmetry-dependent force balance of the walker system and from the symmetry properties of the friction laws, which relate the friction force to the normal contact force and to the sliding velocity on each contact point. In determining the force balance, we

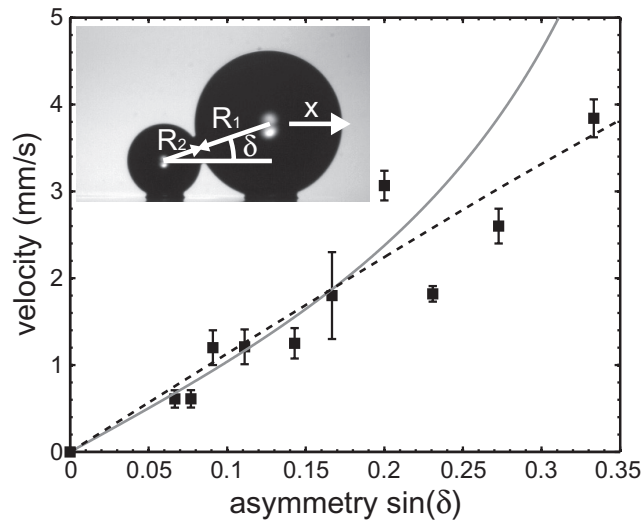


Figure 3. Inset: schematic view of a walker composed of two spheres with radii R_1 and R_2 . Its asymmetry is characterized by the angle δ formed by connecting the centres of the spheres with the horizontal. The vibration axis of the substrate is denoted as x . Main panel: the walkers' velocity as a function of the asymmetry parameter $\sin \delta = (R_1 - R_2)/(R_1 + R_2)$ (squares). The walkers were constructed from precision spheres with 0.2, 0.25, 0.3, 0.35 and 0.4 mm radii on a glass prism. The vibration frequency was fixed at 80 Hz and the dimensionless force Γ_0 was kept fixed at 0.5. The error bars represent the range of data resulting from multiple experimental measurements. The grey solid curve shows the expected theoretical dependence of the walkers' velocity on the asymmetry parameter $\sin \delta$ from our model with a linear friction law (theory supplement, equation (S9)) where $\kappa = 0.032 \text{ s mm}^{-1}$. The dashed black line represents the expected average velocity for a friction law with a Coulomb and a viscous friction term, computed numerically with $\mu = 0.24$ and $\alpha = 550$. The fit parameters have the same value as in figure 2 for both theory curves.

assume that the two beads remain in contact with each other and the substrate. This geometrical constraint imposes an asymmetry dependent relationship between the friction forces and the normal contact forces that act on the beads. Using a quasi-static approximation gives an expression of the friction forces as simple functions of the dimensionless force Γ . Finally, the friction laws provide the link between the friction and normal forces and the sliding velocities, and thus the locomotion velocity, as will be discussed in more detail below.

We consider a walker, composed of two spherical beads with radii R_1 and R_2 and masses m_1 and m_2 , which are held together and attached to a flat horizontal substrate by adhesive forces provided by liquid bridges. The walker is subjected to an external driving force that is parallel to the substrate. When the walker is aligned with the direction of the excitation, the plane defined by the three contact points is the plane of symmetry of the system (see figure 4), and all of the forces lie within that plane. The beads can rotate and slide on the substrate and on each other. The angular velocity of sphere i about an axis perpendicular to the symmetry plane is denoted by $\dot{\varphi}_i$, and its sliding velocity on the substrate is denoted by v_i . The sliding

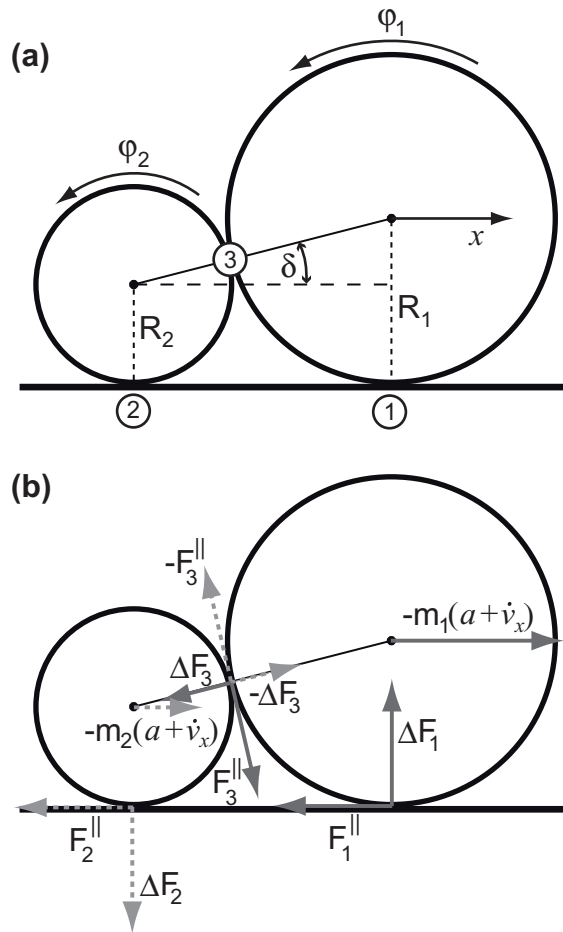


Figure 4. (a) Side view of a walker composed of two spherical beads on a flat horizontal substrate, aligned with the shaking direction (the x -axis). The circled numbers define the indices corresponding to the three points of contact. The angular velocities $\dot{\varphi}_i$ are considered to be positive in the counterclockwise direction, and the velocity of the walker on the substrate v_x is considered to be positive from left to right, as indicated by the arrow. (b) Sketch representing, with arrows, the friction forces F_i^{\parallel} and the net normal forces ΔF_i that act on the three contact points, and the inertial forces that act on the centre of mass of the beads. All force vectors lie in the plane of symmetry of the system. The solid dark grey arrows correspond to forces that act on bead 1, while the dashed light grey arrows correspond to forces that act on bead 2. The inertial forces are considered positive when they point from bead 2 towards bead 1. The friction forces are considered to be positive in the direction opposite to the positive sliding velocities, and so in this sketch F_1^{\parallel} and F_2^{\parallel} are positive, whereas F_3^{\parallel} is negative. The resulting normal forces ΔF_i are positive when they point towards the centre of the bead to which they apply.

velocity of bead 1 on bead 2 is thus $v_3 = R_1\dot{\varphi}_1 + R_2\dot{\varphi}_2$. Assuming that the spheres remain in hard mechanical contact with each other and the substrate, such that the geometry of the walker does not change over time, the velocity of the centre of mass of both beads and of the walker

with respect to the substrate is described by a single variable along the shaking direction, $v_x = v_1 - R_1\dot{\phi}_1 = v_2 - R_2\dot{\phi}_2$. The acceleration of the structure with respect to the substrate is denoted by \dot{v}_x .

We first describe the forces that act on the two beads in the rest frame of the walker, which holds true as long as contact is maintained at each contact point. In our experiments, the substrate is subjected to a harmonic mechanical vibration with an acceleration $a(t) = a_0 \cos(2\pi ft)$ in the reference frame of the lab. Consequently, the driving force consists of the inertial forces acting on the beads, where the inertial force $-m_i(a(t) + \dot{v}_x(t))$ is acting on the centre of mass of bead i . Adhesive forces act on each contact point and are normal to the contact plane. Given that their direction is fixed, they can be represented in a compact form by using the three-component vector notation $\mathbf{F}^a := (F_1^a, F_2^a, F_3^a)$, where F_i^a is the magnitude of the adhesive force exerted on bead i at the contact point i with the substrate (for $i \in \{1, 2\}$), and F_3^a is the magnitude of the adhesive force exerted on bead 1 at the contact point 3 between the two beads. In our experiments, the adhesive forces are capillary forces and can be written as [17, 18]

$$\mathbf{F}^a = -k_0 \bar{R} \begin{pmatrix} 1 + \sin \delta \\ 1 - \sin \delta \\ \frac{1}{2} \cos^2 \delta \end{pmatrix}, \quad (1)$$

where $k_0 = 4\pi\gamma$. The average radius $\bar{R} = \frac{1}{2}(R_1 + R_2)$ characterizes the length scale of the system, $\sin \delta = (R_1 - R_2)/(R_1 + R_2)$ characterizes the asymmetry of the system, and the characteristic magnitude of the adhesive forces, $k_0 \bar{R}$, sets the typical force scale of the system. The minus sign on the right-hand side of equation (1) arises from our sign convention. Note that van der Waals adhesive forces could be written in the same form simply by defining $k_0 = A/12\epsilon^2$, where A is the Hamaker constant and ϵ is a cutoff parameter, which may be identified with surface roughness [18]. The weight of bead i acts on its centre of mass in the vertical direction with an amplitude $-m_i g$, where g is the acceleration due to gravity. The beads also experience two types of contact forces at each contact point: contact forces normal to the plane of contact that are elastic in origin and resist the indentation of the surfaces, and friction forces within the plane of contact that resist the relative motion of the surfaces. The direction of the contact forces is thus solely determined by the geometry of the system. Their amplitudes are represented by F_i for the normal contact and F_i^{\parallel} for the friction forces that are exerted by the substrate on the bead i (for $i \in \{1, 2\}$), F_3 for the normal contact force and F_3^{\parallel} for the friction force exerted by bead 2 on bead 1 at the contact point 3. The magnitudes of the contact forces are written in the three-component vector notation as $\mathbf{F} := (F_1, F_2, F_3)$ and $\mathbf{F}^{\parallel} := (F_1^{\parallel}, F_2^{\parallel}, F_3^{\parallel})$. The friction forces are considered to be positive in the direction opposite to the positive sliding velocities.

At rest (when there is no driving force), there are no friction forces, and the system is in mechanical equilibrium due to the presence of the normal contact forces \mathbf{F}^0 that oppose the adhesive forces and the weight of the beads. Since the ratio of the weight of a spherical bead to the capillary force adhering it to the substrate, $m_i g/k_0 R_i = \rho g R_i^2/3\gamma$, is ≤ 0.1 for all of the systems we have investigated, we further neglect the weight of the beads relative to the adhesive forces between the beads and the substrate. The normal contact forces are then simply balancing the adhesive forces given by equation (1), such that

$$\mathbf{F}^0 = -\mathbf{F}^a. \quad (2)$$

Under driving ($a \neq 0$), when the beads are subjected to an inertial driving force, the friction forces are nonzero and the normal contact forces change from their value at rest to become

$$\mathbf{F} = \mathbf{F}^0 + \Delta\mathbf{F}. \quad (3)$$

As long as contact is maintained at each contact point, the variation in the normal contact forces $\Delta\mathbf{F}$, which are the resulting forces acting on the contact points in the normal direction after summing the adhesion forces with the normal contact forces, can be derived from the balance of forces in the rest frame of the walker, as illustrated in figure 4(b). In the presence of an inertial driving force in the x -direction, the balance of forces acting on bead 1 gives

$$\begin{aligned} F_3^{\parallel} \cos \delta + \Delta F_1 + \Delta F_3 \sin \delta &= 0, \\ \Delta F_3 \cos \delta - m_1(a + \dot{v}_x) - F_1^{\parallel} - F_3^{\parallel} \sin \delta &= 0, \end{aligned} \quad (4)$$

where \dot{v}_x is the acceleration of the structure with respect to the substrate. The balance of forces acting on the walker gives

$$\Delta F_1 + \Delta F_2 = 0 \quad (5)$$

and

$$F_1^{\parallel} + F_2^{\parallel} + M(a + \dot{v}_x) = 0, \quad (6)$$

since there is no net force acting on contact point 3 according to Newton's third law. Using equations (4)–(6), the normal contact forces can then be written as

$$\mathbf{F} = \mathbf{F}^0 + \frac{1}{\cos \delta} \begin{pmatrix} -\frac{1-\mathcal{M}}{2} \sin \delta & \frac{1+\mathcal{M}}{2} \sin \delta & -1 \\ \frac{1-\mathcal{M}}{2} \sin \delta & -\frac{1+\mathcal{M}}{2} \sin \delta & 1 \\ \frac{1-\mathcal{M}}{2} & -\frac{1+\mathcal{M}}{2} & \sin \delta \end{pmatrix} \mathbf{F}^{\parallel}. \quad (7)$$

This relationship depends only on the asymmetry of the walker through the angle δ and the relative mass difference of the spheres $\mathcal{M} = (m_1 - m_2)/M$.

In the quasi-stationary limit, an approximation whose application is validated by the fact that no frequency dependence has been observed in the walkers' velocities, the rate of change of the rolling velocities of the beads on the substrate, $R_i \dot{\varphi}_i$, and the acceleration of the walker on the substrate \dot{v}_x are negligible with respect to the acceleration of the substrate in the reference frame of the lab, a . An expression for the rate of change of the sliding velocities of the spheres comprising a walker in the general case is given in the theory supplement, section 1.1 (available from stacks.iop.org/NJP/13/053041/mmedia). In the quasi-static limit, a constant angular velocity $\dot{\varphi}_i$ for both of the spheres means that the overall torque due to the friction forces applied on bead i has to be equal to zero (as represented in figure 4(b)). As a result, and given our sign convention,

$$F_1^{\parallel} = -F_3^{\parallel} = F_2^{\parallel}. \quad (8)$$

Similarly, a constant locomotion velocity means that equation (6) becomes

$$F_1^{\parallel} + F_2^{\parallel} = -Ma. \quad (9)$$

After normalizing all of the forces by the force scale $k_0 \bar{R}$ given by the adhesive forces, the combination of equations (8) and (9) gives

$$\frac{\mathbf{F}^{\parallel}}{k_0 \bar{R}} = \frac{\Gamma}{2} \begin{pmatrix} -1 \\ -1 \\ 1 \end{pmatrix}. \quad (10)$$

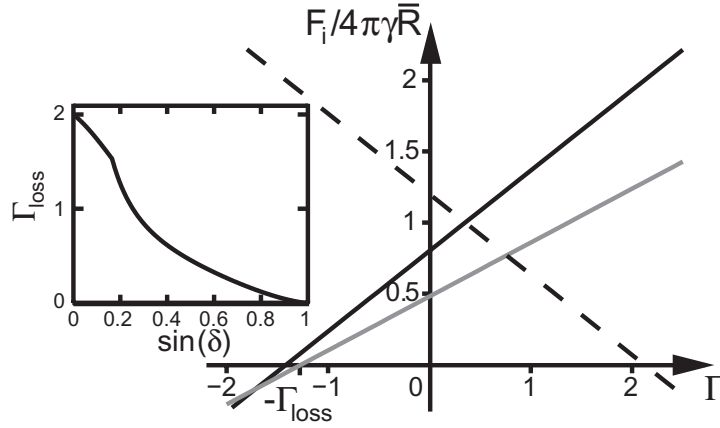


Figure 5. Theoretical dimensionless normal forces $F_i/4\pi\gamma\bar{R}$ as a function of the dimensionless force Γ , calculated from equation (11) for a walker with $\sin\delta = 0.2$. Dashed line: $i = 1$; solid black line: $i = 2$; grey line: $i = 3$. Inset: magnitude of the dimensionless force at which the first contact is lost, Γ_{loss} , as a function of the asymmetry parameter $\sin\delta$.

Hence, the friction force on each contact point, normalized by the force scale $k_0\bar{R}$, is proportional to the dimensionless driving force $\Gamma(t)$. As a result, the normal contact force on each contact point given by equation (7) and normalized by $k_0\bar{R}$ is an affine function of Γ , as depicted in figure 5,

$$\frac{\mathbf{F}}{4\pi\gamma\bar{R}} = \begin{pmatrix} 1 + \sin\delta \\ 1 - \sin\delta \\ \frac{1}{2}\cos^2\delta \end{pmatrix} + \frac{\Gamma}{2\cos\delta} \begin{pmatrix} -\mathcal{M}\sin\delta - 1 \\ \mathcal{M}\sin\delta + 1 \\ \mathcal{M} + \sin\delta \end{pmatrix}. \quad (11)$$

Finally, the friction law on each contact point relates the friction force F_i^{\parallel} to the normal contact force F_i and the sliding velocity v_i . It is typically an odd function of the sliding velocity v_i [19, 20], such that

$$F_i^{\parallel}(F_i, -v_i) = -F_i^{\parallel}(F_i, v_i). \quad (12)$$

According to equation (10), the friction force F_i^{\parallel} is also an odd function of the dimensionless driving force Γ , and so we must have

$$F_i^{\parallel}(F_i(-\Gamma), v_i(-\Gamma)) = -F_i^{\parallel}(F_i(\Gamma), v_i(\Gamma)) \quad (13)$$

for any Γ value. Since the normal forces do not have any special symmetry with respect to Γ (see equation (11) and figure 5), the sliding velocities v_i cannot, in general, be odd functions of Γ if the relationship in equation (13) is to be respected. Indeed, if the sliding velocity v_i were an odd function of Γ , and the relationship in equation (12) were satisfied, it would require that the relationship $F_i^{\parallel}(F_i(-\Gamma), v_i(\Gamma)) = F_i^{\parallel}(F_i(\Gamma), v_i(\Gamma))$ is fulfilled for any Γ value. This is not generally true when $F_i(-\Gamma) \neq F_i(\Gamma)$, and so the sliding velocities v_i cannot be odd functions of Γ . As a result, for a periodic and symmetric driving force $\Gamma(t)$, the average value of the sliding velocity at each contact point is typically nonzero, as is the average velocity of the walker. When

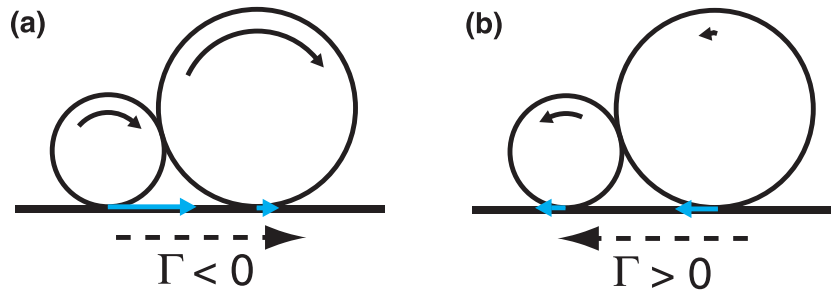


Figure 6. Sketch representing the motion of a walker with a linear friction law in the rest frame of the substrate during: (a) a forward stroke ($\Gamma < 0$), and (b) a backward stroke ($\Gamma > 0$) with the same amplitude as the forward stroke but the opposite direction. The dashed arrows indicate the direction of the inertial driving forces that act on the walker. The curved black arrows represent the rolling velocity of the beads on the substrate, $-R_i\dot{\phi}_i$. The straight blue arrows represent the sliding velocity of the beads on the substrate. The small bead is both rolling and sliding during the forward and the backward strokes, whereas the big bead is mainly rolling during the forward stroke, and mainly sliding during the backward stroke. The total velocity of the beads is larger during the forward stroke than during the backward one, which leads to locomotion in the direction of the large sphere during a driving cycle.

an explicit expression for the friction law on each contact point is given, the sliding velocity v_i can be calculated as a function of the peak dimensionless force Γ_0 and the asymmetry of the walker, δ , by using the expressions for the friction force F_i^{\parallel} and the normal force F_i given by equations (10) and (11), respectively. Finally, the walker's velocity v_x is a linear combination of the sliding velocities of the three contact points, $v_x(\Gamma, \delta) = \frac{1}{2}(v_1 + v_2 - v_3)$, and its average value over one excitation period can be quantitatively compared with the experimental data. In the following section, we consider two types of friction laws: a simple linear friction law and a friction law that contains Coulomb and viscous friction terms.

4. Discussion

A basic picture of the mechanism of motion of the walker can be drawn by considering a simple, fully linear friction law of the form $F_i^{\parallel} = \kappa v_i F_i$. In the reference frame of the substrate, when $\Gamma < 0$ and the inertial force is directed towards the large bead (see figure 6(a)), the forward sliding motion of the large bead is impeded by an increase in the normal contact force F_1 on the contact between the large bead and the substrate (figure 5, dashed line). At the same time, the forward rotational motion of both beads is enhanced by the decrease in the normal force F_3 between the two beads, which facilitates the sliding of one bead over the other (figure 5, grey line). The forward sliding of the small bead is also enhanced by the small value of the normal force F_2 between the small bead and the substrate (figure 5, black line). Conversely, when $\Gamma > 0$ and the inertial force is directed towards the small bead (see figure 6(b)), the backward sliding motion of the large bead is facilitated by the decrease in the normal force F_1 , but the increased values of the normal forces F_3 and F_2 impede both the backward rotation motion of the beads and the backward sliding motion of the small bead. In this case, the small bead acts like a brake

for both the rolling and the sliding motion directed towards the small bead. Due to this braking action, the distance travelled during the backward stroke, $\Gamma > 0$, is smaller than the distance travelled during the forward stroke, $\Gamma < 0$, when the forward rolling motion is enhanced. This results in an overall locomotion in the direction of the large sphere.

To compare the model with our experimental data, we calculated the average value of the velocity of the walker v_x , with the linear friction law mentioned above applied to all three contact points, and for a harmonic excitation $\Gamma_0 \cos(2\pi ft)$. Averaging over one period, we obtained a function of the peak dimensionless force Γ_0 and the asymmetry δ ; the average velocity, \bar{v}_x , is plotted with the experimental data in figures 2 and 3 as grey curves (the explicit expression is given in the theory supplement, equation (S9)). In order to fit this expression to our data, the walker's asymmetry parameter $\sin \delta$ was set to the value of 0.2 in figure 2, and the dimensionless force Γ_0 was set to 0.5 in figure 3, in correspondence with the experimental parameters. The single fit parameter $\kappa = 0.032 \text{ s mm}^{-1}$ was used in both figures. In figure 3, the theoretical velocity dependence of the walker on the asymmetry parameter $\sin \delta$ is consistent with the experimentally observed trend. In particular, the locomotion velocity vanishes as the asymmetry parameter goes to zero. However, the theoretical velocity prediction deviates from the experimental dependence on the peak dimensionless force Γ_0 displayed in figure 2 at low and high values, since neither the threshold for motion at low dimensionless force nor the plateau region are reproduced using the simple linear friction law.

A better agreement with the experimental features is obtained when a more standard friction law that includes both Coulomb and viscous friction terms is used: $F_i^{\parallel} = \mu F_i v_i / |v_i| + \alpha \eta \bar{R} v_i$, where μ is the coefficient of sliding friction, α is a dimensionless geometrical factor and η is the dynamic viscosity of the wetting fluid. In this case, the average walkers' velocity over one period of harmonic driving $\Gamma(t) = \Gamma_0 \cos(2\pi ft)$ was computed numerically. Our method of solving this system numerically is described in detail in the theory supplement (available from stacks.iop.org/NJP/13/053041/mmedia). The average walkers' velocity is compared with the experimental data in figures 2 and 3 (black dashed curves), using the fit parameters $\mu = 0.24$ and $\alpha = 550$, where the value we obtained for the sliding friction coefficient μ is a reasonable value for our system [20]. A threshold for the onset of motion at a low dimensionless force and a plateau at higher dimensionless forces are both reproduced. The threshold for the onset of motion is due to the Coulomb friction term, as the sliding velocity v_i remains equal to zero as long as $|F_i^{\parallel}| \leq \mu |F_i|$. The dimensionless force thresholds for the onset of sliding on each contact point depend on the asymmetry of the walker, the friction coefficient μ , and the direction of the sliding motion. Motion is only possible when the magnitude of the dimensionless peak force Γ_0 becomes larger than the lowest threshold for the onset of sliding on one of the contact points, Γ_c . For a walker with $\sin \delta = 0.2$ and $\mu = 0.24$, our model gives $\Gamma_c = 0.19$, a predicted value that is close to the experimental threshold for the onset of motion displayed in the inset of figure 2. For a dimensionless peak force $\Gamma_0 > \Gamma_c$, the walker switches between different modes of motion as the dimensionless force Γ varies, each time a threshold for the onset of sliding is crossed. These Γ -dependent modes of motion are responsible for the different regimes of the theoretical walker's velocity versus Γ_0 curve: an initial sharp increase in the velocity for $\Gamma_0 > \Gamma_c$, a plateau at intermediate Γ_0 values, and a further increase for yet higher peak dimensionless forces. A more detailed analysis of the rich dynamical behaviour predicted with this model is beyond the scope of this article because the modes of motion of the walker, and the boundaries of these modes in parameter space, depend sensitively on the specific friction law used on each contact point.

Directed motion was predicted by means of both types of friction laws we have implemented, even the fully linear one. Even if the details of the friction laws are important for describing the specifics of the walkers' modes of motion, these details do not matter much for *some kind* of directed motion to occur. In our theoretical description, the ratchet phenomenon itself is very robust in the sense that for it to occur, it is simply required that the friction force F_i^{\parallel} depends on the normal contact force F_i and is an odd function of the sliding velocity v_i (such that $F_i^{\parallel}(F_i, -v_i) = -F_i^{\parallel}(F_i, v_i)$), which is usually true for real contacts [19, 20].

The key asymmetry in our model comes from the relationship between the normal forces and the friction forces given by equation (7). This relationship was obtained under the condition that the beads remain in contact with each other and the substrate throughout the excitation cycle. The essential role of the adhesive forces in this system is to maintain contact against the driving force, which is why the adhesive forces define the relevant force scale in the system ($4\pi\gamma\bar{R}$ for capillary forces of a perfectly wetting fluid). Contact between the beads and the substrate is maintained as long as the peak dimensionless force Γ_0 remains below the smallest dimensionless force in absolute value, Γ_{loss} , for which one of the normal contact forces becomes equal to zero and the corresponding contact is lost (see figure 5). The value of Γ_{loss} , calculated *a posteriori* using equation (11), only depends on the asymmetry of the walker $\sin\delta$ and is plotted in the inset of figure 5; its expression is given in the theory supplement section 1.2. For a walker with $\sin\delta = 0.2$, as in figure 2, Γ_{loss} is equal to 1.2. This value is very close to the peak dimensionless force where the experimental walker's velocity drops off in figure 2, $\Gamma_0 \approx 1.1$, and so we surmise that this velocity decrease is due to loss of contact in the system.

Another striking feature of the experimental system is that the walkers first self-align, then remain aligned with the direction of the excitation, while migrating across the substrate. In order to understand the stability of the walker's direction of locomotion, we consider the sideways motion of the walker in the plane of the substrate, when it is not perfectly aligned with the shaking direction (see the theory supplement, section 2, available from stacks.iop.org/NJP/13/053041/mmedia). Let ψ be the angle between the axis passing through the contact points 1 and 2 between the beads and the substrate and the direction of the applied oscillation (illustrated in the theory supplement figure S2). If the pair of beads roll sideways without sliding, and the walker's acceleration associated with locomotion is small relative to the acceleration of the substrate, the dynamics of the angle ψ are equivalent to the motion of a parametric pendulum. For small angles ψ and a harmonic driving force oscillating with a frequency f , the equation of motion for sideways rolling reduces to a differential equation of Mathieu type [21]. Defining the dimensionless time variable $\vartheta = \pi ft$, this equation can be written in canonical form as

$$\frac{d^2\psi}{d\vartheta^2} + [U - 4V \cos(2\vartheta)]\psi = 0, \quad (14)$$

where the parameter U is proportional to the time-averaged driving force, so here $U = 0$. Our system thus dwells on the abscissa of the stability diagram in the (V, U) plane, whose central interval $[-0.45; +0.45]$ lies within a stable region [21], where the stability diagram is shown in figure 7. The parameter V characterizes the amplitude of the parametric oscillation; its expression is given in the theory supplement (equation (S18)). It can be shown that $|V| < 0.4$ for all of the experimental systems investigated in this work, which is well within the stable region. Damping of the rolling motion, which is not accounted for in this description but should

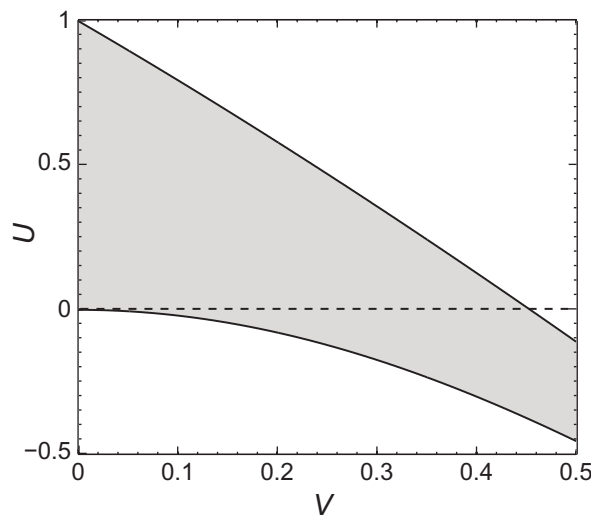


Figure 7. Stability diagram of Mathieu equation (14). It is symmetric about the U axis. The white space corresponds to regions of instability, while the grey shaded area represents the region of stability. The presence of damping is known to enlarge the shaded region [21, 22].

be present in reality, is known to enlarge the stable regions, and to lead to a decrease in the amplitude of the orientation oscillations with time [22]. This explains the self-alignment of the walkers with the direction of the excitation.

5. Conclusion

We have reported the discovery of a novel ratchet system that is able to self-assemble, self-aligns in the driving direction and is robust in that it functions under a wide range of experimental conditions. This ratchet system has been quantitatively studied using artificially assembled asymmetric dimers and we have presented a basic model of this system that successfully reproduces the main experimental features of this system. The basic ingredients of this model are the geometry of the system, a set of friction laws that depend on both the sliding velocity and the normal contact force, and the ratio between the driving and adhesion forces. The source of the rectification mechanism was identified as the asymmetry introduced by the relationship between the friction forces and the adhesive forces; however, the mechanism itself does not rely on the exact nature of the adhesive forces. This suggests that similar effects could be expected in a downscaled system, with adhesion provided by van der Waals forces instead of capillary forces, if a suitable driving method is implemented. We have also shown that the walkers display a rich dynamical behaviour, with several modes of motion predicted; investigating the occurrence and stability of these modes both experimentally and numerically remains a topic for further study.

Acknowledgments

The authors thank Udo Krafft for technical assistance, Elisabeth Charlaix and Mario Scheel for insightful discussions, and Jonathan Bodenschatz and Michael Wiedecke for help with the setup. ZSK acknowledges a fellowship from the Alexander von Humboldt foundation.

References

- [1] Hänggi P and Marchesoni F 2009 Artificial Brownian motors: controlling transport on the nanoscale *Rev. Mod. Phys.* **81** 387–442
- [2] Snezhko A, Belkin M, Aranson I S and Kwok W K 2009 Self-assembled magnetic surface swimmers *Phys. Rev. Lett.* **102** 118103
- [3] Wright H S, Swift M R and King P J 2008 Migration of an asymmetric dimer in oscillatory fluid flow *Phys. Rev. E* **78** 036311
- [4] Dreyfus R, Baudry J, Roper M L, Fermigier M, Stone H A and Bibette J 2005 Microscopic artificial swimmers *Nature* **437** 862–5
- [5] Browne W R and Feringa B L 2006 Making molecular machines work *Nat. Nanotechnol.* **1** 25–35
- [6] den Toonder J *et al* 2008 Artificial cilia for active micro-fluidic mixing *Lab. Chip* **8** 533–41
- [7] Zhang L, Abbott J J, Dong L, Kratochvil B E, Bell D and Nelson B J 2009 Artificial bacterial flagella: fabrication and magnetic control *Appl. Phys. Lett.* **94** 064107
- [8] Mahmud G *et al* 2009 Directing cell motions on micropatterned ratchets *Nat. Phys.* **5** 606–12
- [9] Chang S T, Paunov V N, Petsev D N and Velev O D 2007 Remotely powered self-propelling particles and micropumps based on miniature diodes *Nat. Mater.* **6** 235–40
- [10] Snezhko A, Aranson I S and Kwok W K 2006 Surface wave assisted self-assembly of multidomain magnetic structures *Phys. Rev. Lett.* **96** 078701
- [11] Buguin A, Brochard F and de Gennes P G 2006 Motions induced by asymmetric vibrations *Eur. Phys. J. E* **19** 31–6
- [12] Blair D L, Neicu T and Kudrolli A 2003 Vortices in vibrated granular rods *Phys. Rev. E* **67** 031303
- [13] Dorbolo S, Volfson D, Tsimring L and Kudrolli A 2005 Dynamics of a bouncing dimer *Phys. Rev. Lett.* **95** 044101
- [14] Kudrolli A, Lumay G, Volfson D and Tsimring L S 2008 Swarming and swirling in self-propelled polar granular rods *Phys. Rev. Lett.* **100** 058001
- [15] Rosato A, Strandburg K J, Prinz F and Swendsen R H 1987 Why the brazil nuts are on top: size segregation of particulate matter by shaking *Phys. Rev. Lett.* **58** 1038–40
- [16] Fingerle A, Roeller K, Huang K and Herminghaus S 2008 Phase transitions far from equilibrium in wet granular matter *New J. Phys.* **10** 053020
- [17] McFarlane J S and Tabor D 1950 Adhesion of solids and the effect of surface films *Proc. R. Soc. A* **202** 224–43
- [18] Israelachvili J 1991 *Intermolecular and Surface Forces* (London: Academic Press)
- [19] Olsson H, Åström K J, Canudas de Wit C, Gäfvert M and Lischinsky P 1998 Friction models and friction compensation *Eur. J. Control* **4** 176–95
- [20] Ludema K C 2000 *Modern Tribology Handbook* vol 1, ed B Bushan (Boca Raton, FL: CRC Press) pp 205–34
- [21] McLachlan N W 1947 *Theory and Application of Mathieu Functions* (Oxford: Clarendon Press)
- [22] José J V and Saletan E J 1998 *Classical Dynamics a Contemporary Approach* (Cambridge: Cambridge University Press) pp 424–9